Engineering Notes

ENGINEERING NOTES are short manuscripts describing new developments or important results of a preliminary nature. These Notes cannot exceed 6 manuscript pages and 3 figures; a page of text may be substituted for a figure and vice versa. After informal review by the editors, they may be published within a few months of the date of receipt. Style requirements are the same as for regular contributions (see inside back cover).

Noise of Counter-rotation Propellers with Nonsynchronous Rotors

D. B. Hanson* and C. J. McColgan†
Hamilton Standard, Windsor Locks, Connecticut

Nomenclature

B = number of blades in each rotor
B_D = blade chord-to-diameter ratio
c_0 = ambient speed of sound
C_{Lk} = lift coefficient at loading harmonic k
J_n = Bessel function
M_T = tip rotational Mach number
r,θ,ϕ = observer coordinates ($\theta=0$ on forward axis)
t = time
z_0 = radius ratio of source
Ω_1,Ω_2 = angular speed of front and rear rotors, respectively

Introduction

REFERENCE 1 gives a general formula for noise of a counter-rotation (CR) propeller with any number of blades and any rpm on each rotor. Only the special case of equal rpm's and equal blade numbers was explored in detail. For this special case, it was shown that all of the steady and unsteady source effects produced noise components at the blade passing frequency (BPF) of one rotor and its harmonics so that no new spectrum frequencies are introduced by counter-rotation operation. However, in noise tests of their Fairey Gannet counter-rotation propeller aircraft, Rolls-Royce opted to run the rotors at slightly different speeds to take advantage of the spectrum-splitting behavior described in Ref. 2 to discriminate between rotor-alone and interaction tones. Upon examination of noise recordings from its own Gannet, Hamilton Standard also found the splitting. The sample plots shown in Fig. 1 were measured using "zoom" spectrum analysis.

Theoretical Background

The observed spectrum behavior can be explained by examination of Eq. (1) of Ref. 1, which is the radiation formula for loading noise of one rotor of a CR propeller due to steady plus unsteady loading associated with rotor-rotor interaction.

To study the unequal rpm behavior, this equation is reduced to its essentials by setting flight Mach number and blade sweep, offset, and drag to zero. The observer angle measured in the direction of rotor rotation is set to 90 deg without loss of generality, and the source is considered to be chordwise-compact. The acoustic pressure from the radial station z_0 is then

$$p = K \sum_{m=-\infty}^{\infty} \sum_{k=-\infty}^{\infty} \exp\{i[(m-k)B\phi + (m\Omega_2 + k\Omega_1)B(r/c_0 - t)]\} \times k_y C_{Lk} J_{(m-k)B}[(m + k\Omega_1/\Omega_2)Bz_0 M_T \sin\theta] \quad (1)$$

where

$$k_x = 2BB_D(m-k)/z_0 \quad (2)$$

$$k_y = -2BB_D M_T(m + k\Omega_1/\Omega_2)\cos\theta \quad (3)$$

and K is a collection of constants

Now we further consider the two rotor rpm's to be nearly equal by setting $\Omega_1 = (1+\epsilon)\Omega_2$. This small speed difference of $\epsilon\Omega_2$ will be important in the phase terms of Eq. (1) but not in the amplitude factors, therefore, we can write

$$p = K \sum_{m=-\infty}^{\infty} \sum_{k=-\infty}^{\infty} \exp\{i[(m-k)B\phi + (m + k(1+\epsilon))\Omega_2 B(r/c_0 - t)]\} \times k_y C_{Lk} J_{(m-k)B}[(m+k)Bz_0 M_T \sin\theta] \quad (4)$$

where

$$k_x = 2BB_D(m-k)/z_0 \quad (5)$$

$$k_y = -2BB_D(m+k)\cos\theta \quad (6)$$

Equation (4) is expressed as a sum of spinning modes with mode indices m and k. The frequency and spin rate of a mode are given by the exponential, the mode efficiency by the Bessel function, and the source strength by $k_y C_{Lk}$. Spectrum behavior can be deduced by studying these factors.

The (radian) frequency of a mode is given by

$$\omega_{mk} = |m + k(1+\epsilon)|B\Omega_2 \quad (7)$$

its spin rate by

$$\dot{\phi} = [(m + k(1+\epsilon))/(m-k)]\Omega_2 \quad (8)$$

and its modal efficiency by

$$\eta = J_{(m-k)B}[(m+k)Bz_0 M_T \sin\theta] \quad (9)$$

If we consider noise near the plane of rotation ($\sin\theta \approx 1$) from the blade tip ($z_0 \approx 1$), then the Bessel function argument is $(m+k)BM_T$. The radiation efficiency is related to the ratio between the Bessel function argument and the index.

$$\xi = |(m+k)/(m-k)|M_T \quad (10)$$

For $\xi > 1$, the mode has about unit efficiency; for $\xi < 1$, the efficiency drops rapidly with decreasing ξ. The ξ parameter is similar to the cutoff ratio used in fan analysis.

Application of Theory to Gannet Spectrum

The preceding information was used to generate Tables 1 and 2, which show the behavior of the modes with frequencies near BPF and 2BPF (BPF = blade passing frequency).

Received July 1, 1985; revision received Aug. 21, 1985.

*Principal Research Engineer. Member AIAA.
†Analytical Engineer. Member AIAA.

Table 1 Mode properties at frequencies near BPF

Mode indices		Frequency,	Cutoff ratio,	Spin rate,	Number of lobes,	Modal efficiency,
m	k	$\omega_{m,k}$	ξ	$\dot{\phi}$	$\lvert m-k\rvert/B$	η^a
0	±2	$(2+2\epsilon)B\Omega_2$	M_T	$-(1+\epsilon)\Omega_2$	$2B$	0.057
±1	±1	$(2+\epsilon)B\Omega_2$	∞	∞	0	0.15
±2	0	$2B\Omega_2$	M_T	Ω_2	$2B$	0.057
±3	∓1	$(2-\epsilon)B\Omega_2$	$M_T/2$	$((2-\epsilon)/4)\Omega_2$	$4B$	1×10^{-6}
±4	∓2	$(2-2\epsilon)B\Omega_2$	$M_T/3$	$((1-\epsilon)/3)\Omega_2$	$6B$	3×10^{-13}

[a] $\eta = J_{(m-k)B}[(m+k)Bz_0M_T\sin\theta]$ calculated for $B=4$, $z_0=1$, $M_T=0.8$, $\theta=70$ deg.

Table 2 Mode properties at frequencies near 2BPF

Mode indices		Frequency,	Cutoff ratio,	Spin rate,	Number of lobes,	Modal efficiency,
m	k	$\omega_{m,k}$	ξ	$\dot{\phi}$	$\lvert m-k\rvert/B$	η^a
0	±2	$(2+2\epsilon)B\Omega_2$	M_T	$-(1+\epsilon)\Omega_2$	$2B$	0.057
±1	±1	$(2+\epsilon)B\Omega_2$	∞	∞	0	0.15
±2	0	$2B\Omega_2$	M_T	Ω_2	$2B$	0.057
±3	∓1	$(2-\epsilon)B\Omega_2$	$M_T/2$	$((2-\epsilon)/4)\Omega_2$	$4B$	1×10^{-6}
±4	∓2	$(2-2\epsilon)B\Omega_2$	$M_T/3$	$((1-\epsilon)/3)\Omega_2$	$6B$	3×10^{-13}

[a] $\eta = J_{(m-k)B}[(m+k)Bz_0M_T\sin\theta]$ calculated for $B=4$, $z_0=1$, $M_T=0.8$, $\theta=70$ deg.

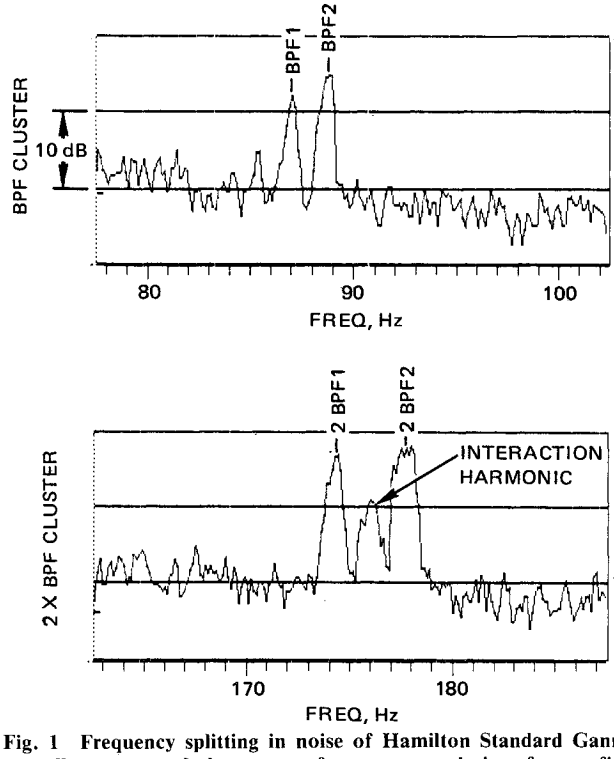

Fig. 1 Frequency splitting in noise of Hamilton Standard Gannet propeller measured by zoom frequency analysis of near-field microphone data.

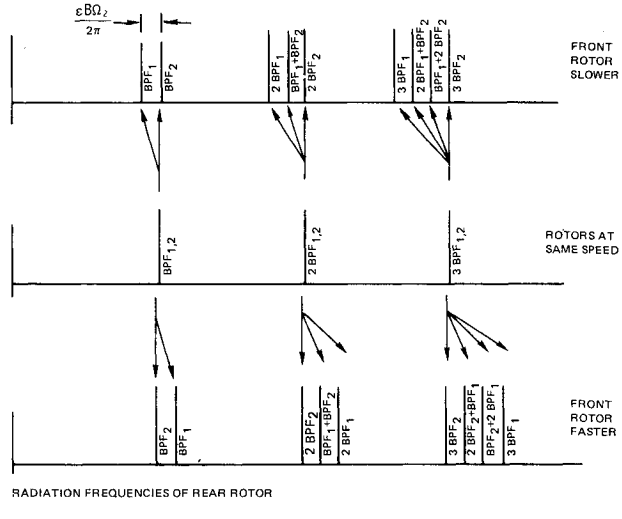

Fig. 2 Frequency-splitting behavior for noise from the rear rotor.

For frequencies near BPF (radian frequency $B\Omega_2$), Eq. (7) shows that only the combinations of m and k which need to be considered are those such that $m+k=1$. These are shown in Table 1. From the modal efficiencies in the last column, it is apparent that only two modes are in contention; namely, for $m,k=0$, ±1 and ±1, 0. The second of these is simply the steady loading effect and appears at frequency $B\Omega_2$, i.e., BPF of rotor 2 (R_2). The other mode, associated with the first unsteady loading harmonic, has frequency $(1+\epsilon)B\Omega_2 = B\Omega_1$, which BPF of R_1. These are the only two frequencies that can radiate from R_2 due to rotor-rotor interaction. Other possible effects on the Gannet at R_1 are steady sources and unsteady loading due to aircraft-fixed distortion which radiates at $B\Omega_1$, and unsteady loading at R_2 due to aircraft-fixed distortion which radiates at $B\Omega_2$. Finally, a table such as Table 1 for rotor-rotor interaction radiating from R_1 would show frequencies $B\Omega_1$ and $B\Omega_2$. Thus it is concluded that the only two frequencies that will appear are the BPF of each rotor. Table 1 shows that the steady and unsteady loading modes have the same efficiency, therefore, the unsteady loading would have to be very strong to be important at BPF. In Fig. 1, the two peaks have roughly the same strength suggesting roughly equal contributions from each rotor.

Table 2 gives the modal properties for frequencies in the 2BPF cluster. Here there are three modes with non-negligible efficiencies. The ±2, 0 mode is due to steady loading on R_2 and appears at 2BPF of R_2, as expected. The 0, ±2 mode associated with the second unsteady loading harmonic appears at frequency $(2+2\epsilon)B\Omega_2 = 2B\Omega_1$, namely, 2BPF of R_1. The ±1, ±1 mode has frequency halfway between at $(2+\epsilon)B\Omega_2 = B\Omega_1 + B\Omega_2$. Arguments similar to those given above show that these are the only frequencies that can appear in the 2BPF cluster. The last column in Table 2 shows that the first unsteady loading mode (±1, ±1) is three times as efficient as steady loading. That is, if the $k=1$ unsteady loading harmonic were one-third of the steady loading, the middle noise spectrum peak would have the same level as the BPF peak from R_2. The noise pattern associated with the $k=1$

loading has 0 lobes, corresponding to the dread plane wave pattern in duct acoustics. Thus, it can be seen that running with an rpm differential gives direct diagnostic information otherwise not available by simple measurement methods.

It should be pointed out that a related diagnostic scheme was developed by Abdelhamid[3] in a ducted rotor experiment with simulated inlet guide vanes (IGV). He rotated the IGV assembly slowly to split the IGV interaction spectrum peaks from those due to other inflow disturbances.

The arguments presented above can be continued to higher harmonics with results shown in Fig. 2. In each BPF harmonic cluster, the highest and lowest peaks will be dominated by steady sources on the faster and slower rotors, respectively. Peaks in between are due to unsteady aerodynamic interaction.

Conclusion

This mode-splitting behavior provides a powerful technique for noise source diagnosis in counter-rotation propellers and should be used in any noise tests where an rpm differential is possible.

References

[1]Hanson, D. B., "Noise of Counter-rotation Propellers," *Journal of Aircraft*, Vol. 22, July 1985, pp. 609-617.

[2]Personal communication with Dr. Andrew Kempton of Rolls-Royce Acoustic Group, Oct. 16, 1984.

[3]Abdelhamid, A. N., "Acoustic Response of a Model Ducted Rotor to Inflow Fluctuations," AIAA Paper 74-89, Jan. 1974.

Stresses Around Holes in Pin-Loaded Orthotropic Plates

M.W. Hyer*
University of Maryland, College Park, Maryland
and
E.C. Klang†
University of Illinois, Champaign-Urbana, Illinois

Introduction

IT was the purpose of the work reported herein to stay within the context of a two-dimensional analysis and study the effects of pin elasticity, clearance, and friction on the stress distributions around the hole in a pin-loaded orthotropic plate. The problem has direct application to the study of composite bolted joints and was studied for that purpose. The pin was considered as a second elastic body that interacted with the plate through contact. The pin, which exerts a net force on the hole edge, was represented by an elastic inclusion within the hole. In reality, the portions of the pin outside the thickness of the plate transmit, through shear, the load to the portion of the pin within the thickness of the plate.

Presented as Paper 84-0915 at the AIAA/ASME/ASCE/AHS 25th Structures, Structural Dynamics and Materials Conference, Palm Springs, CA, May 14-16, 1984; received June 4, 1984; revision submitted Aug. 13, 1985.

*Professor, Department of Mechanical Engineering; formerly, Department of Engineering Science and Mechanics, Virginia Polytechnic Institute and State University, Blacksburg, VA. Associate Fellow AIAA.

†Research Associate, Department of Theoretical and Applied Mechanics.

In this study, since the shear stress across a cross-sectional area of the pin is nearly uniform, the effect of the shear stress was represented by a uniform in-plane body force acting on the elastic inclusion. With this two-dimensional approach, the pin elasticity being considered was an across-the-diameter elasticity. Complex variable elasticity, along with a numerical procedure, were used to find a solution to the problem. The numerical procedure consisted of collocation, to enforce the boundary conditions around the hole, and iteration, to find the contact and no-slip regions between the plate and pin. A complete discussion of the theory and the numerical procedure can be found in Ref. 1. With the analysis, the effects of pin modulus, friction levels, and degrees of clearance between the pin and plate could be assessed within the framework of the theory of elasticity. The problem was treated as a two-dimensional problem, as opposed to a three-dimensional one, to assess the effect of pin elasticity, friction, and clearance in the context of all the previous analyses that approached the problem as two-dimensional. With this approach, the seriousness of ignoring clearance, for example, in past analyses could be quantified. More importantly, composite bolted-joint design criteria based on a two-dimensional analysis and material failure data appear to give reasonable results when compared with test results.[2] Thus, a two-dimensional analysis has value. However, by using a two-dimensional approach, bolt-bending effects, clamping force (torque-up) effects, and interlaminar stresses cannot be accounted for.

Numerical Results

Numerical results were computed in order to assess the effects of the various parameters on the stresses around the hole. The results reported on here are for a $[0_2/\pm 45]_s$ graphite-epoxy laminate with the following material properties:

$$E_x = 85.5 \text{ GPa}, \qquad E_y = 25.7 \text{ GPa}$$

$$G_{xy} = 22.1 \text{ GPa}, \qquad \nu_{xy} = 0.667 \text{ GPa}$$

This represents a laminate with a moderate level of orthotropy, $E_x:E_y = 3:1$.

Figure 1 shows the effects of pin elasticity on the stresses around the hole edge. Three pin flexibilities are illustrated: a rigid pin ($E = \infty$), a steel pin ($E = 207$ GPa), and an aluminum pin ($E = 68.9$ GPa). Poisson's ratio of the pin had very little effect on the numerical results. A value of 0.3 was used. Figure 1

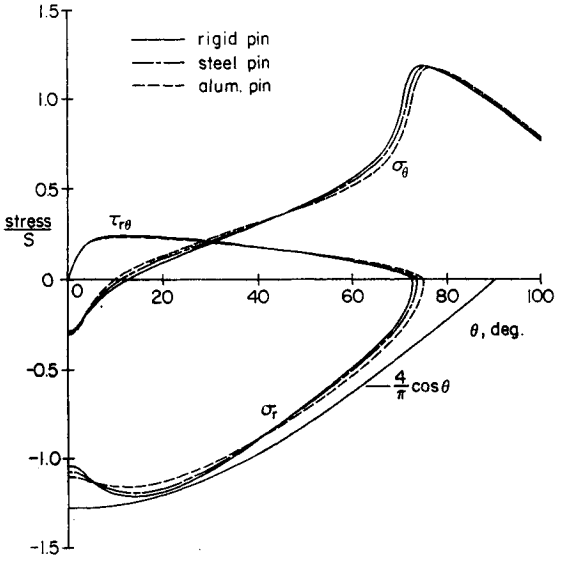

Fig. 1 Effect of pin elasticity on stresses around hole.